

Antiprotonic studies of nuclear neutron halos

S. Wycech,^{*} J. Skalski,[†] and R. Smolańczuk[‡]
Sołtan Institute for Nuclear Studies, Hoża 69, PL-00-681, Warsaw, Poland

J. Dobaczewski[§]
Institute of Theoretical Physics, Warsaw University, Hoża 69, PL-00-681, Warsaw, Poland

J. R. Rook
Particle and Nuclear Physics Laboratory, University of Oxford, Oxford, United Kingdom

(Received 10 October 1995; revised manuscript received 26 June 1996)

Nuclear capture of antiprotons from atomic states is studied. Partial widths for single-nucleon capture events leading to cold residual nuclei are calculated. Recent CERN experiments that compare the neutron and proton captures are analyzed. Nuclear density distributions at the extreme nuclear surface are calculated and tested against the experimental results. [S0556-2813(96)04410-X]

PACS number(s): 25.43.+t, 21.10.Ft, 21.10.Gv

I. INTRODUCTION

Recent CERN experiments with antiprotonic atoms [1] have renewed interest in the question of the comparison of the proton and neutron density distributions in the surface region of large nuclei. It has been known for years that hadronic, in particular kaonic, atoms provide a means by which the extreme tail of the nuclear density distribution may be studied including the isospin structure and nuclear correlations [2]. Two methods have been used [3–9], each of which gives information in the region roughly 2.0 fm beyond the half density radius: (1) observation of the x-ray cascade in hadronic atoms and extraction from the resulting data of the atomic level widths and shifts and (2) studies of the particles, particularly mesons, emitted following the capture of the hadron.

Method (1) provides only very limited information since for most nuclei only one level width and shift can be measured. Method (2) can in principle provide much more information; particularly it can differentiate captures on protons from those on neutrons. Unfortunately, it has proved difficult to obtain reliable information as a result of uncertainties concerning both the initial capture states and the final state interactions.

The new experiments of Ref. [1], involving antiprotons, have two very strong advantages. First, they differentiate reasonably clearly between the $\bar{p}p$ and $\bar{p}n$ annihilations, thus ensuring that the neutron and proton distributions can be separately estimated. Second, they involve antiproton absorption which is more distant from the nuclear half-density radius than the earlier experiments mentioned above. We shall show that the absorption occurs in a region around 3.0 fm beyond the half-density radius.

The idea of the experiments of Ref. [1] is to detect

“cold” nuclei, following the absorption of antiprotons in antiprotonic atoms, by radiochemical methods. By “cold” here we mean nuclear states of very low energy, less than the neutron emission threshold. Characterizing a nucleus of N neutrons and Z protons by (N, Z) the reactions are

$$(A) \quad \bar{p} + (N, Z) \rightarrow (N, Z-1) + \text{mesons},$$

$$(B) \quad \bar{p} + (N, Z) \rightarrow (N-1, Z) + \text{mesons}.$$

Thus (A) involves predominantly interactions of the \bar{p} with protons and (B) similarly with neutrons. It is the possibility of distinguishing reactions (A) and (B) experimentally which is the first advantage of the method of this paper using the experiments of Ref. [1].

The extreme surface nature of the process considered here arises first from the high orbital angular momentum of the \bar{p} , but this is well known and was exploited in earlier experiments [3–9]. The new circumstance, which points to an even more peripheral character of the considered reaction, is the detection of final nuclei *in spite* of meson production in (A) and (B). On the average there are four to five mesons emitted and to leave a final $Z-1$ or $N-1$ nucleus they must all avoid collision with it. This can happen only if the annihilation takes place at the far nuclear surface.

The basic $N\bar{N}$ interactions are needed for the study of this paper. They are limited by several phenomenological parameters: the range of the $N\bar{N}$ annihilation, absorptive parts of the scattering amplitudes, pion production multiplicities, and pion momentum distributions. These are taken from other experiments but the effects of the uncertainties must be quantified. Once the final and initial states are understood one can interpret the ratio of processes (A) and (B) in terms of “neutron halos” or “neutron skins” and attribute quantitative meaning to these terms. Qualitatively, we shall see that the analysis of the CERN experiments [1] shows a large neutron excess at the nuclear surface of several heavy nuclei. This result complements similar findings in the sub-Coulomb neutron pickup reactions [10].

One purpose of this paper is to provide a description of the nuclear capture of the atomic antiprotons. Of main interest is the fraction of single-nucleon captures which leaves

^{*}Electronic address: WYCECH@FUW.EDU.PL

[†]Electronic address: JSKALSKI@FUW.EDU.PL

[‡]Electronic address: SMOLAN@FUW.EDU.PL

[§]Electronic address: DOBACZEW@FUW.EDU.PL

cold nuclei in the various final states corresponding to capture by protons and neutrons. Difficulties in the way are two-fold. First, the $N\bar{N}$ annihilation is a complicated process with many degrees of freedom involved. Second, the initial atomic state of the antiproton and the final states of the residual nuclei are not certain. Fortunately, the importance of the first difficulty is much reduced as a result of the large energy release in the \bar{p} absorption. As a result, a closure approximation over nuclear final states together with high energy approximations for the annihilation mesons may be applied, yielding classical formulas for the absorption rates. The latter are expressed by integrals of nuclear densities weighted by a probability to find the antiproton inside the nucleus and by a probability to find the final nucleus left undestroyed by the annihilation products. The last two probabilities are calculated on the basis of the antiproton and pion optical potentials. Their dependence on the initial atomic state, final state interactions, and parameters of the \bar{p} and pionic nuclear optical potentials is studied in Sec. II.

In Sec. III, the experimental data of Ref. [1] is used to obtain information concerning neutron halos. It is necessary to use detailed models for the nuclei involved and we consider four such models. These are the Fermi gas, shell model, Hartree-Fock, and Hartree-Fock-Bogolyubov (HFB) models. Comparison of the experimental data of Ref. [1] with these models is described and the situation concerning the neutron halo discussed. The advantages and limitations of the method are indicated.

II. NUCLEAR ABSORPTION OF ATOMIC ANTIPROTONS

Antiprotons bound into atomic orbits cascade down the atomic levels to be ultimately absorbed by the nucleus. The latter happens at the extreme nuclear surface and the absorption probability is significant even at distances as large as twice the nuclear radius [3,8,9]. Two effects create such a situation. First, the mean free path of antiprotons in nuclear matter is less than 1 fm, and second, the atomic cascade tends to populate states of high angular momentum l . The peripherality of capture allows the use of standard low density simplifications: quasifree scattering and a single-particle picture of the nucleus. It also facilitates the description of the final mesons, a vital point in understanding the absorption experiments of Ref. [1]. On the other hand, the disadvantage and difficulty inherent in studies of the nuclear surface are related to the sensitivity to range effects.

This section presents a description of the antiproton absorption mechanism. First, a simple phenomenological picture based on the optical potential model is presented. Next, two special questions—final state interactions and range effects—are discussed, again in a phenomenological way. A more detailed justification of the phenomenological approach, including its basic assumptions and limitations, is given in two consecutive subsections. These consist of a rather technical discussion which may be omitted by readers more interested in the nuclear structure results.

The tool to describe the antiprotonic atomic level shifts and widths is an antiproton-nucleus optical potential V^{opt} . The simplest one is usually [8,9,11] assumed to have the form

$$V^{\text{opt}}(\mathbf{R}) = \frac{2\pi}{\mu_{N\bar{N}}} t_{N\bar{N}} \rho(\mathbf{R}), \quad (1)$$

where $\mu_{N\bar{N}}$ is the reduced mass, $\rho(\mathbf{R})$ is a nuclear density at a radius \mathbf{R} , and $t_{N\bar{N}}$ is a complex scattering length. As the range of the $N\bar{N}$ interaction is finite the density $\rho(\mathbf{R})$ involved in Eq. (1) is assumed not to be the ‘‘bare’’ nuclear density $\rho_0(\mathbf{R})$ but a folded one:

$$\rho(\mathbf{R}) = \int d\mathbf{u} \rho_0(\mathbf{R}-\mathbf{u}) v(\mathbf{u}), \quad (2)$$

where v is a form factor that represents the $N\bar{N}$ force range. For the absorptive part of V^{opt} an annihilation range of 1 fm might be expected from models of the $N\bar{N}$ annihilation but the range in the real part is more uncertain.

The length $t_{N\bar{N}}$ in Eq. (1) is extracted from antiprotonic atomic data. The most precise x-ray measurements have been done for the $3d$ and $4f$ states in the oxygen isotopes [8,9], and fits to these give $t_{N\bar{N}}$ of about $-1.5-i2.5$ fm [11,12]. This value yields a deep and strongly absorptive optical potential. At the nuclear center $\text{Im}V^{\text{opt}}$ would be 200 MeV and the related mean free path would be well below 1 fm. However, it should be kept in mind that both the form and the strength of V^{opt} are tested only in the surface region of nuclei. In particular, $\text{Im}V^{\text{opt}}$ is determined by the atomic level widths Γ via

$$\Gamma = 4 \frac{\pi}{\mu_{N\bar{N}}} \text{Im} t_{N\bar{N}} \int d\mathbf{R} \rho(\mathbf{R}) |\Psi_{\bar{N}}(\mathbf{R})|^2, \quad (3)$$

where $\Psi_{\bar{N}}(\mathbf{R})$ is the atomic wave function. Since only atomic states of high angular momenta l are available and $\Psi_{\bar{N}} \approx R^l$, the absorption strength is peaked at the surface.

The nuclear absorption scenario is visualized in Fig. 1(a) for the nucleus ^{58}Ni which, as the simplest one to describe, will be our reference case. We show the R dependence of the integrand in Eq. (3), $W = \rho |\Psi_{\bar{N}}|^2 R^2$. The surface nature of the \bar{p} capture is seen there in more detail, confirming the qualitative arguments just projected.

The capture of the \bar{p} by the atom and the subsequent cascade through the \bar{p} atomic levels are a consequence of processes which are difficult to describe in detail. The simplest description is that the cascade is entirely through the ‘‘circular’’ orbits, i.e., those with principal quantum number $n = \ell + 1$. This assumption is far too extreme in detail but is sufficient for our purposes as the dominant feature we require is the value of ℓ for the \bar{p} and not the value of n . The reason for this is that the \bar{p} atomic wave functions in the region of the nucleus are dominated by the value of ℓ . Henceforth we consider only circular atomic orbits.

There are two special atomic states singled out in the capture process. One is the so-called ‘‘upper’’ level which usually is the last one that can be detected before the cascading \bar{p} is absorbed. One can learn the width of this upper state by measuring the intensity loss of the x-ray transitions. In ^{58}Ni , and in many other nuclei, the nuclear absorption is most likely to happen from this level. The next circular state below is called the ‘‘lower’’ one. Sometimes, one can measure the shape of the x-ray lines feeding this lower state.

TABLE I. Atomic results. Columns 2 and 3 contain the principal quantum number n and the angular momentum l . For the remaining columns: c.p. is the nuclear capture probability calculated under the assumption that the circular atomic state $n = n_{\text{upper}} + 1$ is fully occupied, $\sigma_{A-1} = \Gamma^{A-1}/\Gamma^{\text{tot}}$ is the branching ratio for the cold capture, and $\sigma_{np} = \Gamma_n/\Gamma_p$ is the ratio of captures on neutrons to protons. The AD model and $R_{np} = 0.63$ were used.

Element	n	l	c.p.	σ_{A-1}	σ_{np}
^{58}Ni	4	3	0	0.095	0.69
	5	4	0.16	0.097	0.69
	6	5	0.83	0.110	0.70
	7	6	0.01	0.150	0.71
	8	7	0	0.220	0.71
^{96}Zr	6	5	0.24	0.106	4.67
	7	6	0.72	0.128	5.30
^{130}Te	7	6	0.05	0.096	1.77
	8	7	0.93	0.122	2.00
^{144}Sm	7	6	0.01	0.075	1.39
	8	7	0.75	0.085	1.46
^{154}Sm	7	6	0.01	0.087	3.65
	8	7	0.75	0.099	3.98
^{176}Yb	8	7	0.23	0.097	3.34
	9	8	0.75	0.124	4.07
^{232}Th	7	6	0	0.073	3.94
	8	7	0	0.091	4.64
	9	8	0.31	0.098	5.00
^{238}U	10	9	0.69	0.127	6.20
	9	8	0.29	0.106	6.55
	10	9	0.71	0.138	8.24

Such measurements are possible only when the width of the lower state is in the range of a few keV and, additionally, the rate of radiation from the upper state is comparable with the absorption rate from that state. The capture probabilities from several circular states are given in Table I. The lower state widths are usually larger than the upper state widths by two orders of magnitude. That is due to the smaller orbit radii and reduced centrifugal barriers. However, the absorption density profile is not changed dramatically as may be seen from the ratio of these densities given in Fig. 1(a). Hence the possibility of capture from the lower level is not expected to affect our subsequent conclusions.

The localization of nuclear capture in the surface region depends on the range of the NN forces. One way to find this range is to use NN potential models. Another, perhaps more advantageous, is to fit the atomic and low energy scattering data. An early choice was to use charge density profiles for the ρ [8,9,11]. This is equivalent to folding a form factor $\nu(\mathbf{u})$ in Eq. (2) with a rms radius of 0.8 fm. More recently, Gaussian profile form factors $\exp[-(r/r_0)^2]$ with longer range have been used [12,13]. Typical best fit values are $r_{0i} \approx 1$ fm (for $\text{Im}V$) and $r_{0r} \approx 1.5$ fm (for $\text{Re}V$). On the other hand, calculations based on the NN potentials yield average ranges r_{0i} of 0.75 fm up to 1.45 fm [14,15], the differences being due to different handling of the off-shell extensions. An effect of the range is shown in Fig. 1(a). A longer NN absorption radius broadens the region of nuclear absorption. The related effect on the n/p ratio is shown in Fig. 1(b) and discussed later.

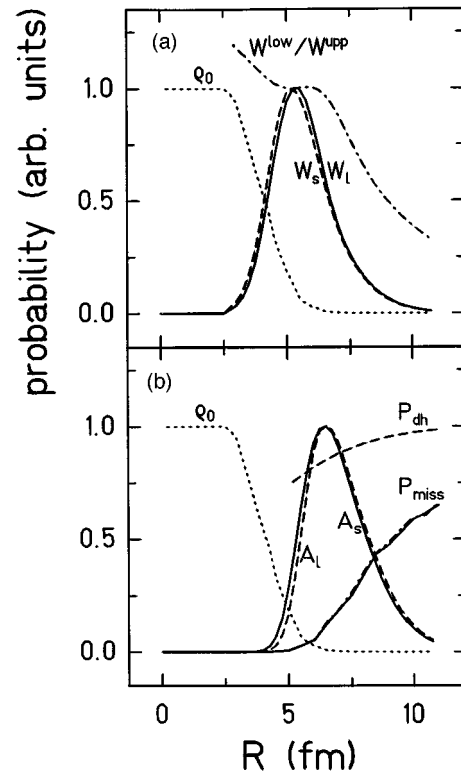


FIG. 1. (a) The total antiproton absorption densities from the “upper” $n=6$, $l=5$ orbit in ^{58}Ni : W_l for the NN annihilation range $r_0=1$ fm and W_s for the range $r_0=0.75$ fm. The dot-dashed line is a ratio of two W_l for subsequent circular $n=5$ and $n=6$ atomic states. ρ_0 is a “bare” neutron density. Normalizations are arbitrary. (b) The $(A-1)$ “cold” antiproton absorption density on a neutron from $n=6$ circular orbit in ^{58}Ni . A_l given by the integrand of Eq. (4) for the NN annihilation range $r_0=1$ fm and A_s for the range $r_0=0.75$ fm. ρ_0 is a “bare” neutron density. Normalizations are arbitrary. Missing probabilities (left scale): P_{miss} , solid line, is due to phase space alone, and P_{miss} , dash-dotted line, is calculated with corrections for the experimental pion momentum distribution. The flat dashed curve is P_{dh} from the HFB model.

Optical model calculations based on the NN interaction potentials [14,16–18] indicate that the lengths t_{NN} required in such calculations bear no simple relation to the empirical S -wave NN scattering lengths. The latter give an optical potential with a repulsive real part while empirically it is attractive. The conclusion is that $\text{Re}t_{NN}$ is of a complicated and uncertain structure. At the extreme nuclear surface it reflects a long attractive tail of the pion exchange forces, and about the nuclear radius it may turn to repulsion due to repulsive scattering lengths and is rather uncertain at nuclear matter densities. On the other hand, the phenomenological best fit to $\text{Im}t_{NN}$ represents the cumulative effect of the S - and P -wave absorptive amplitudes, and can be well understood in terms of the free $\text{Im}t_{NN}$. The calculated optical potentials indicate a structure more complicated than that given by formula (1), but cannot reproduce the data as accurately as the latter with empirical best fit parameters. As a result, in this calculation we use the phenomenological approach. The level widths discussed so far reflect all modes of the nuclear absorption of antiprotons. The initial stage, an elementary

$N\bar{N}$ annihilation, generates an energy of 2 GeV, of which 3/4 is the kinetic energy taken by the final state mesons. The mesons may excite the residual nucleus via inelastic scattering and absorption. To calculate the total widths one sums over the unobserved nuclear excited states. The large energy release and peripherality allow us to use closure over the nuclear states. As a consequence, the effective $\text{Im}t_{N\bar{N}}$ is close to the absorptive part of the free $N\bar{N}$ scattering amplitude. That is no longer true when the final nuclear states are limited to some particular states, as is the case of the experiments of Ref. [1] in which radiochemical methods were used to detect ‘‘cold’’ nuclei. In these experiments, final nuclei excited up to the neutron separation threshold only can be detected. Residual nuclei of higher excitations would decay by a neutron emission before being detected by the radiochemistry. In the next subsections, the spectrum of allowed excited states is related to the rearrangement of the nucleons within the nucleus and to the interactions of the final state mesons.

Now, to explain our aim, we give a simplified result which will be proven and refined later. Let s denote the quantum numbers of the annihilated nucleon (neutron or proton), the antiproton atomic orbital (n, l, j) , and the final state of the residual nucleus (any nucleus or cold nucleus). We are going to prove a simple expression for the partial absorption width Γ_s corresponding to the ‘‘cold’’ nucleus formation. In the limit of the zero-range force this reads

$$\Gamma_s = 4 \frac{\pi}{\mu_{N\bar{N}}} \text{Im}t_{N\bar{N}}^s \int d\mathbf{R} |\Psi_{N\bar{N}}(\mathbf{R})|^2 \rho_s(\mathbf{R}) P_s(\mathbf{R}). \quad (4)$$

In this expression, a function P_s is introduced to describe the formation of the required final states. It is a product of two terms $P_s = P_{\text{miss}} \times P_{\text{dh}}$. The dominant factor in P_s is P_{miss} , the probability that the mesons originating at point \mathbf{R} do not excite the residual nucleus (missing probability of Ref. [1]). The other final state factor P_{dh} is related to the final nucleus rearrangement and happens to be less significant. Examples of these functions are given in Fig. 1(b). The integrand in Eq. (4), including the R^2 factor, is the absorption density for those processes that lead to cold $(A-1)$ residual nuclei. It is shown as A in Fig. 1(b). In comparison to the full absorption density W given in Fig. 1(a) it is shifted to the periphery by almost 1 fm. It is this shift which enhances the surface nature of the process measured in Ref. [1] and makes it particularly interesting for studies of nuclear surfaces.

Now, we derive Eq. (4), calculate P_{miss} , P_{dh} , and hence P_s , and study the effects of the finite range of $N\bar{N}$ interaction.

A. Nuclear $N\bar{N}$ annihilation and final state interactions

The aim of this section is to calculate the rate of nuclear $N\bar{N}$ annihilations that lead to cold final nuclei. This is done in several steps.

(1) An amplitude for the $N\bar{N}$ annihilation into mesons $t_{N\bar{N} \rightarrow M}$ is assumed and introduced into the nuclear transition amplitude in the impulse approximation.

(2) The meson emission probabilities are calculated and summed over the mesonic and nuclear final states. For an isolated $N\bar{N}$ annihilation this procedure would produce the

absorptive cross section and, via the unitarity condition, the absorptive amplitude $\text{Im}t_{N\bar{N}}$. For nuclear captures leading only to cold nuclei we limit the summation over final states to the states of elastic meson-nucleus scattering. This limited summation generates an effective $\text{Im}t_{N\bar{N}}$ again, but now it is folded over nuclear factors due to the final state interaction of the mesons.

(3) To simplify our considerations, effects related to the finite range of the reaction—propagation of the final mesonic resonances, recoil effects, nonlocalities due to external fields, and the size of the mesonic source—are discussed at the end of this section.

Assume that an antiproton in an atomic state characterized by quantum numbers collectively denoted by n annihilates on a nucleon in a single-particle state α into k mesons with momenta p_i , $i=1-k$. In the impulse approximation, the transition amplitude for this process is

$$A_{n,\alpha} = \int \Psi_{N\bar{N}}^n(\mathbf{x}) \varphi_N^\alpha(\mathbf{y}) t_{N\bar{N} \rightarrow M}(\mathbf{x}, \mathbf{y}, \xi) \prod_i \bar{\varphi}_M(\mathbf{p}_i, \xi_i, \beta), \quad (5)$$

where $\Psi_{N\bar{N}}(\mathbf{x})$ is the atomic, $\varphi_N(\mathbf{y})$ the nuclear, and φ_M the mesonic wave functions. The latter describes scattering states and corresponds to the ingoing boundary condition. The final state of the nucleus is not specified; in the spirit of the impulse approximation it is the initial nucleus that is left with a hole in the single-particle state α . Additional nuclear excitations follow nonelastic interactions of the mesons. States generated in this way are denoted by an index β in the mesonic wave functions.

The transition amplitude $t_{N\bar{N} \rightarrow M}(\mathbf{x}, \mathbf{y}, \xi)$ is not known in detail. What one needs for atomic studies is, basically, the elastic $\text{Im}t_{N\bar{N}}^s$ extended to the off-shell region. The momentum extension is related to the range dependence, expressed in terms of the $N\bar{N}$ relative coordinate $\mathbf{x}-\mathbf{y}$. As already discussed, this is fairly well known, contrary to the range dependence in the mesonic coordinates ξ . The kinematic conditions are special since both the N and \bar{N} are bound and the pair energies fall below the $N\bar{N}$ threshold. Even at these energies, the nuclear momenta reach $1-2 \text{ fm}^{-1}$ and the scattering matrix should include at least S and P waves with all possible spin states. The relevant partial cross sections or partial absorptive amplitudes $\text{Im}t_{N\bar{N}}$ could be calculated from potential models of the $N\bar{N}$ scattering. Such a procedure is adopted in some optical potential calculations [14,16–19], even though the partial wave analysis of the $N\bar{N}$ scattering does not exist. Unfortunately, the problem discussed here is more involved and uncertainties are larger. We aim, rather, at a semiphenomenological ‘‘effective $\text{Im}t_{N\bar{N}}^s$ ’’ as used in the phenomenological optical potential.

To calculate the absorption widths, we take the square modulus of the amplitudes (5), sum over the final pionic channels, and integrate over the phase space. We also sum over the final nuclear states and in this way arrive at an expression for the partial absorption widths Γ_s ,

$$\Gamma_s = 4 \frac{\pi}{\mu_{N\bar{N}}} \int \Psi_{N\bar{N}}(\mathbf{x}) \varphi_N^\alpha(\mathbf{y}) I^s(\mathbf{x}, \mathbf{y}, \mathbf{x}', \mathbf{y}') \bar{\Psi}_{N\bar{N}}(\mathbf{x}') \bar{\varphi}_N^\alpha(\mathbf{y}'), \quad (6)$$

where

$$I^s = \sum_{\beta} \sum_k \int dL \int d\xi \int d\xi' t_{NN \rightarrow M}^s(\mathbf{x}, \mathbf{y}, \xi) \varphi_M(\mathbf{p}, \xi, \beta) \times \bar{\varphi}_M(\mathbf{p}, \xi', \beta) t_{NN \rightarrow M}^s(\xi', \mathbf{x}', \mathbf{y}'). \quad (7)$$

Here, the integration dL runs over pionic Lorentz-invariant phase space restricted by the energy conservation and k is the pion multiplicity. For an isolated NN system, at or below the threshold, I^s in Eq. (7) is related by unitarity to the absorptive part of the elastic NN scattering amplitude

$$I^s = \text{Im} t_{NN}^s(\mathbf{x} - \mathbf{y}, \mathbf{x}' - \mathbf{y}') \delta(\mathbf{R} - \mathbf{R}'), \quad (8)$$

where $\mathbf{R} = (\mathbf{x} + \mathbf{y})/2$ is the NN center-of-mass coordinate.

For an annihilation inside the nucleus this free space unitarity relation is not true since, in the external field, the propagation of the intermediate particles in Eq. (7) changes. If Eq. (8) is a good approximation, then the \bar{p} optical potential is directly related to t_{NN}^s . Detailed calculations [14,16–19] show that, in the surface region, the optical potential is indeed related to t_{NN}^s but it is not the case in the nuclear interior. As we are only interested in the surface region appropriate closure approximations may still be made. The vital point is the restriction of possible processes to those leaving the nucleus in a state of low excitation. First we discuss the chance that the mesons created in the \bar{p} annihilation would leave the residual nucleus in such a state. Another excitation mode, the rearrangement, is discussed afterwards.

The spectrum of mesons consists essentially of pions of which a sizable fraction is correlated into ρ and ω resonances. These heavy mesons have substantial energy width and after some 1 fm propagation range turn into pions. The multiplicity of pions ranges from 2 to 8 with an average 4–5, and the average momentum is as large as 2 fm^{-1} . Nuclear interactions of these pions may be absorptive, inelastic, or elastic. Those involving a pion absorption occur on two or more nucleons and hence produce $(A - 2)$ or lighter nuclei. The inelastic processes end up with excited nuclei. These may be the $(A - 1)$ nuclei of interest since the dominant mechanisms involve single-nucleon excitation modes: Δ and higher resonances. For medium and heavy nuclei, and pionic energies around the energy of the Δ , the inelastic cross sections reach 0.5 b [20]. However, the main strength is located much higher than the neutron emission threshold. Below this threshold, cross sections are typically 1–10 mb [21]. On the other hand, the elastic cross sections are very large and reach 1 b [20]. Hence, the rate for production of cold nuclei is given essentially by the elastically scattered waves. We shall see that this enables us to use an optical potential description. In addition, in the bulk of the phase space, the pions are fast enough to allow an eikonal description. Following this, the wave function for each pion is taken in the form

$$\bar{\varphi}_M^{(-)}(\mathbf{p}\xi) = \exp[i\mathbf{p}\xi - iS(\mathbf{p}, \xi)], \quad (9)$$

with S calculated in terms of the pion-nucleus optical potential,

$$S(\mathbf{p}, \xi) = \int_0^\infty ds \left[\sqrt{\left(p^2 - U^{\text{opt}} \left(\xi + \frac{\mathbf{p}}{p} s \right) \right) - p} \right]. \quad (10)$$

The function S is calculated in a quasiclassical way by integrating the local momentum over the straight line trajectory. Because of nuclear excitations and pion absorption, this wave is damped with a rate described by $\text{Im}S$. The latter is generated by the absorptive part of the pionic optical potential $\text{Im}U^{\text{opt}}$. This damping follows the whole path of a pion but the main effect comes from regions of large nuclear densities and not from the region around the place of creation, ξ . We assume that all functions $S(\mathbf{p}, \xi)$ are related to the central point of annihilation \mathbf{R} which is the NN c.m. coordinate. Effects of the source size are discussed later, jointly with consequences of the propagation range of the heavy mesons. The assumption that the emission of mesons occurs from the central point substantially simplifies our calculations. With the mesonic wave functions (9), which enter Eq. (7), the total momentum of the mesons \mathbf{P} separates to give a plane wave form. Some additional dependence on \mathbf{P} is still there but, as we show later, it is rather weak. One consequence is that the NN system c.m. ‘‘conservation’’ $\delta(\mathbf{R} - \mathbf{R}')$, which arises in the free unitarity relation (8), is also a good approximation in the nuclear case (7). Now the final state pion interaction factors that enter Eq. (7) may be collected into a function

$$P^k(\mathbf{R}) = \left\langle \prod \left| \exp[-S(\mathbf{p}_i, \mathbf{R})] \right|^2 \right\rangle, \quad (11)$$

which is a product of the eikonal factors within each multiplicity k . It has to be averaged over the multiplicities and the pionic phase space weighted by some unknown momentum dependence generated by the t matrix for NN processes giving mesons, $t_{NN \rightarrow M}$. The expectation is that the momentum dependence of P^k is weak as compared to the momentum dependence of $t_{NN \rightarrow M}$ since the former is determined by the nuclear size and the latter by the size of annihilation region. Thus one may expect the unitarity condition to hold approximately, provided the averages of P^k in Eq. (7) are factored out. This averaging is now performed and in this way one arrives at

$$I^s \approx \text{Im} t_{NN}^s(\mathbf{x} - \mathbf{y}, \mathbf{x}' - \mathbf{y}') \delta(\mathbf{R} - \mathbf{R}') P_{\text{miss}}(\mathbf{R}), \quad (12)$$

where the ‘‘missing probability’’ is given by

$$P_{\text{miss}}(\mathbf{R}) = \sum_k w_k \int dL f(p_i) \times \prod \left| \exp[-S(\mathbf{p}_i, \mathbf{R})] \right|^2 / \sum_k w_k \int dL f(p_i). \quad (13)$$

The integration extends over the restricted Lorentz phase space weighted by an experimental multiplicity distribution w_k , for k from 2 to 8 [22,23]. In order to check the assumptions, factors $f(p_i)$ have been introduced into Eq. (13), while pure phase space and constant t matrices correspond to

$f=1$. This probability density selects those pionic interactions that do not excite the residual nucleus.

Calculations of P_{miss} are performed in a Monte Carlo procedure. The optical potential for pions must cover a wide momentum range from the threshold up to 0.9 GeV but the phase space favors a region just above the Δ resonance. This potential is related to the pion-nucleon forward scattering amplitudes and in this way to the pion-nucleon cross sections. That method is well established around the Δ [24]. Here, this procedure is extended to cover also higher resonances N_{11}^* and N_{13}^* which are described by Breit-Wigner amplitudes. The two-nucleon absorption mode is taken in a phenomenological form [25]. Performing these calculations one finds that (1) high energy expansion of the square root in Eq. (10) is satisfactory, (2) higher resonances cannot be neglected, and (3) the black sphere limit is a good approximation in dense regions. In particular, $P_{\text{miss}}(\mathbf{R})$ is changed by less than 10% with an inclusion of the two-nucleon absorption. The latter, being of the ρ^2 profile, operates in the region where the black sphere limit is well fulfilled. An example of calculated $P_{\text{miss}}(\mathbf{R})$, given in Fig. 1(b), is close to a purely geometrical estimate that relates it to the solid angle subtended by the nucleus, as viewed from the point \mathbf{R} [22]. Nevertheless, the gray zone at the nuclear surface makes the effective radius of an equivalent black sphere difficult to predict off-hand.

The $P_{\text{miss}}(\mathbf{R})$ calculated in this way is at best semiquantitative, but the proximity of the strong absorption limit makes the result fairly independent of the details of the annihilation. One question remaining is that the phase space alone does not reproduce the experimental momentum distribution of a single pion [26]. To remove this discrepancy, additional factors $f(p_i)$, which generate the correct distribution, have been introduced into the average (13). The new $P_{\text{miss}}(\mathbf{R})$ is shown in Fig. 1(b). We see that it differs only slightly from the pure phase space result. As the correction procedure is uncertain and the change is below experimental uncertainties we follow the pure averaging procedure over phase space in the remainder of our calculations.

In the surface region of interest, the missing probabilities P_{miss} rise linearly with the distance R . That is a fortunate result. It makes P_{miss} rather insensitive to the size and structure of the annihilation region which is actually located in a small sphere around \mathbf{R} . The same applies to the effects of the ρ and ω mesons. These may propagate some distance to a point \mathbf{R}' and decay into pions there. Those events are approximately confined to within a sphere centered at \mathbf{R} of a radius roughly equal to the particle's velocity multiplied by its lifetime, i.e., ≈ 1 fm. Again, the linearity of $P_{\text{miss}}(\mathbf{R}')$ makes an averaged pionic missing probability equal to $P_{\text{miss}}(\mathbf{R})$.

Let us turn now to other corrections. The annihilation happens at the nuclear surface and is confined to a region of a small diameter. Nevertheless, effects of the nucleus should be considered. These are the $N\bar{N}$ center-of-mass motion, external field, and Pauli principle in the intermediate states. In the far surface region, most of these effects have been found small in optical model calculations. Now we discuss briefly their implications for reactions with a final "cold" $A-1$ nucleus. The first elementary effect, due to the presence of

the nucleus, is the $N\bar{N}$ center-of-mass motion with respect to the residual nucleus. It is given by the recoil energy, i.e., by a Fourier transform of $t_{N\bar{N}}(E-P^2/4M)$ over P , the c.m. momentum in the $N\bar{N}$ system. It is known in kaonic atoms [4,5] that a narrow (30 MeV or less) resonance close to the threshold induces a propagation range as large as 1 fm and affects strongly the peripherality of nuclear capture. Extensive experimental efforts have given no clear evidence for narrow resonances in the $N\bar{N}$ system, close to the threshold. Therefore we assume here that transition matrices $t_{N\bar{N}\rightarrow M}$ are independent of energy. As a result, the annihilation is fast, the c.m. of the $N\bar{N}$ system may be considered fixed in the absorption process, and the factor $\delta(\mathbf{R}-\mathbf{R}')$ is justified in Eq. (12). On the other hand, an effect of the c.m.-motion arises due to the dependence of the pionic functions $S(\mathbf{p}_i, \mathbf{R})$ on the total momentum of mesons \mathbf{P} . It induces some nonlocality in the variable $\mathbf{R}-\mathbf{R}'$ but the effect enters in the second order of a small quantity $P/(\text{pion momentum})$. Numerical studies described earlier indicate a nonlocality of a 0.1 fm range, negligible in comparison to the 1 fm range involved in the relative coordinate $\mathbf{x}-\mathbf{y}$.

B. Range effects

In the limit of zero-range $N\bar{N}$ interactions, the formula (6) for the partial absorption width may be expressed in terms of nuclear densities. For interactions with a finite range, the single-particle wave functions involved may be reduced only to mixed densities. However, for simplicity and historical reasons, one wants to have an approximate expression in terms of the true densities. At the nuclear surface, this can be done with good precision, at least for the absorption rates summed over all nucleon states. The standard relation [27] that allows this is

$$\sum_{\alpha} \bar{\varphi}_i^{\alpha}(\mathbf{y}') \varphi_i^{\alpha}(\mathbf{y}) \approx \rho_i(\mathbf{Y}) j_0[k_F(\mathbf{Y})|\mathbf{y}-\mathbf{y}'|], \quad (14)$$

where $\mathbf{Y}=(\mathbf{y}+\mathbf{y}')/2$, k_F is an effective local Fermi momentum which may be calculated in the shell model, and $i=p$ or n . In a similar way, we express the angular averaged atomic wave functions $\bar{\Psi}\Psi$ by

$$\frac{1}{2l+1} \sum_m \bar{\Psi}_N^n(\mathbf{x}') \Psi_N^n(\mathbf{x}) \approx |\Psi_N^n(\mathbf{X})|^2 \{D^n(\mathbf{X}-\mathbf{X}') + O(\mathbf{X}/nB, \mathbf{X}'/nB)\} \quad (15)$$

which is an expansion in the inverse Bohr radius of the orbit, $1/(nB)$.

Finally, to handle the $N\bar{N}$ interaction range, we assume a separable approximation for the scattering matrix in Eq. (12), $t_{N\bar{N}} = v(\mathbf{x}-\mathbf{y}, r_0\sqrt{2}) t_{N\bar{N}}^0(\mathbf{x}'-\mathbf{y}', r_0\sqrt{2})$, where v are the Gaussian form factors with the range parameter r_0 . This allows for a simple transformation to relative coordinates and reduces Eq. (6) into a folded density expression [14]. For the capture rates one has now

$$\Gamma_s = 4 \frac{\pi}{\mu_{N\bar{N}}} \text{Im} t_{N\bar{N}}^0 \int |\Psi_{N\bar{N}}(\mathbf{Y})|^2 v(\mathbf{Y}-\mathbf{X}, r_0)$$

$$f_X \rho_i(\mathbf{X}) P_{\text{miss}}^s \left(\frac{\mathbf{X} + \mathbf{Y}}{2} \right), \quad (16)$$

where f_X is a factor that collects together a large part of the finite-range effects,

$$f_X = \int d\mathbf{u} v(\mathbf{u}, 2r_0) j_0[k_F(\mathbf{X})\mathbf{u}] D(\mathbf{u}). \quad (17)$$

The factor f_X equals 1 in the limit of zero-range force, with a normalized form factor v . For a typical $N\bar{N}$ absorption range of $r_0 = 1$ fm, values of f_X in the range 0.5–0.6 are obtained. These are almost constant in the nuclear surface region of interest and may be taken out of the integral. As our analysis involves only ratios of the widths, the actual values of f_X are unimportant.

The summation in Eq. (14) selects capture events that lead to single-hole nuclear states. These do not correspond to the experimental conditions which require cold final nuclei or, more precisely, nuclei either in the ground states or in states excited below the neutron emission threshold T_n . To account for this point we limit the sum over the initial nucleon states in Eq. (10) to those that leave the final nucleus with excitation energies less than $T_n + 2$ MeV, where 2 MeV is allowed for neutron kinetic energies. At the surface almost all single-particle (s.p.) states of sizable overlap with the atomic antiprotons contribute to the sum. The experimental cutoff that eliminates deeply bound nucleons becomes a (small) correction, which we call a ‘‘deep hole’’ factor. It is defined as the ratio of a limited sum of single nucleon densities to the total sum, $P_{\text{dh}}(\mathbf{X}) = \frac{\sum_{\alpha}^{\text{ld}} \varphi_{\alpha}^2}{\sum_{\alpha} \varphi_{\alpha}^2}$. When implemented into the partial width formula, it produces

$$\Gamma_s(\text{cold}) = 4 \frac{\pi}{\mu_{N\bar{N}}} \text{Im} t_{N\bar{N}}^0 f_X \int |\Psi_{\bar{N}}(\mathbf{Y})|^2 v(\mathbf{Y} - \mathbf{X}, r_0) \times \rho_j(\mathbf{X}) P_{\text{dh}}(\mathbf{X}) P_{\text{miss}}^s \left(\frac{\mathbf{X} + \mathbf{Y}}{2} \right). \quad (18)$$

This is our result and now we turn to practical, model calculations of the basic ingredients in this equation.

III. CALCULATIONS OF NUCLEAR DENSITIES

For the first test we use an asymptotic density (AD) model for the nucleus. It follows, essentially, the Bethe-Siemens approach [28] but it also incorporates larger phenomenological input, i.e., charge density distribution, neutron and proton separation energies, and the difference between the rms radii of proton and neutron densities. At central densities a Fermi gas of independent protons and neutrons is assumed. The Fermi momenta are determined by the densities and the Fermi energies are fixed by the separation energies. This gives the depth of the potential well which, in the surface region, is extrapolated by the Woods-Saxon form. The densities are given by the exponential damping of the nucleon wave functions due to the potential barriers. For protons a Coulomb barrier is added and potential parameters (half-density radius c and the surface thickness t) are fitted to reproduce the experimental charge density down to 5% of the central density. For neutrons the same t is used while c is

chosen to obtain the rms radius equal (or larger by 0.05–0.10 fm in the heaviest nuclei [29]) to the rms radius of proton density. This model is expected to generate average level densities. Shell effects and correlations are not properly taken care of.

As a second method to determine neutron and proton densities we have used a self-consistent Hartree-Fock (HF) theory with the effective two-body Skyrme-type interaction. Since our aim in using the HF method was rather unusual, i.e., to find nucleon densities at the extreme tails of the nuclear matter distribution (at distances of 8–15 fm from the center), a few remarks about its practical implementation seem to be in order here. The necessary practical condition is the use of a HF code not restricting in any way the asymptotic form of the s.p. wave functions. This condition excludes all codes using the harmonic oscillator basis. In the present work we have applied the code solving the HF equations on the spatial mesh, in which all fields and densities are expressed in the coordinate representation.

The most severe restriction of the results presented is the imposed spherical symmetry. It allows enormous simplification of solution; in particular, the HF equation takes the form of a differential equation in the radial variable for each pair of the conserved s.p. quantum numbers l and j . We used 100 mesh points in the radial coordinate, in a box of the size of 25 fm, and put as a boundary condition that the values of the wave functions at the far end of the box be equal to zero.

The density matrix is obtained by summing contributions from the lowest s.p. orbits. If necessary, the contribution of the last orbit is calculated in the filling approximation; i.e., an appropriate occupation probability, smaller than 1, is associated with this orbit.

The asymptotic form of the radial s.p. wave function for large r corresponding to the s.p. energy eigenvalue ϵ_{nlj} is

$$\mathcal{R}_{nlj}(r) = w_l \left(\frac{1}{r} \right) \exp(-\kappa r)/r, \quad (19)$$

where $\kappa = \sqrt{(2m/\hbar^2)|\epsilon_{nlj}|}$ and w_l is a polynomial with the dominant term being a constant, so that the contribution to the asymptotic density is proportional to $\exp(-2\kappa r)/r^2$. For proton orbitals there is an additional exponential factor, coming from the Coulomb barrier and modifying κ_p , which is very important for distances in question, i.e., between 7 and 15 fm. Although at very large distances from the center the neutron-to-proton density ratio is proportional to $\exp[2(\kappa_p - \kappa_n)r]$, where κ_n and κ_p are directly related to neutron and proton separation energies, respectively, at distances near the \bar{p} absorption peak usually a few neutron and proton orbitals contribute significantly to the density and a more detailed analysis is necessary to evaluate the latter.

Single-particle binding energies (Fermi levels) important in the determination of nuclear density tails are not reproduced exactly with existing effective Skyrme forces. In addition, calculated spherically symmetric densities for deformed nuclei lack quadrupole correlations which *a priori* may for their own sake distort positions of the Fermi levels. Therefore, calculated densities, especially for deformed nuclei, must be treated as approximate, and possible sources of error must be kept in mind. In particular, the true densities of deformed nuclei may have longer tails since, roughly speak-

ing, their elongated form has to be smeared over Euler angles in order to obtain spherically symmetric density in the laboratory frame. A more consistent calculation for deformed even-even nuclei would require a projection of the deformed HF wave function onto zero angular momentum subspace. The projected wave function should then be used to calculate the one-body density. Such a task is still very demanding numerically and beyond the scope of the present study.

In spite of the approximate character of our nuclear density calculations we used also HFB theory [30,31] in order to assess modifications introduced to HF results by the residual pairing interaction. In the present case it must be distinguished from the very often used HF+BCS method, in which the pairing correlations are included using the BCS prescription to self-consistent orbitals. In the latter case, the partial occupation of orbitals above the Fermi level leads to a nonzero, though usually minuscule, occupation of orbitals of positive energy (in the continuum). Since such orbitals are not localized, this implies that they dominate the nuclear density at large distances which is a completely unphysical effect.

The applied HFB code also uses the coordinate representation and the HFB equations are solved on a spatial mesh. The proper analysis of the asymptotic properties of two-component quasiparticle wave functions shows [32] that the HFB ground state wave function, even containing pairing correlations, is always localized if bound. The asymptotic form of the occupied negative-energy quasiparticle states is as in Eq. (19), with κ defined in terms of the sum $E_{nlj} - \lambda$, where E_{nlj} is the quasiparticle energy and λ is the Fermi energy.

As the effective force we use the ten-parameter Skyrme SkP interaction described in Ref. [32]. It has a virtue that the pairing matrix elements are determined by the force itself, contrary to other Skyrme-type interactions which define only the particle-hole channel. In the paired HFB ground state the pairing gap is state dependent. As a simple pairing gap parameter one can use the pairing potential average over the occupied states.

The ‘‘deep hole’’ correction factor in the HFB method is calculated using the additional condition $\epsilon_n < \lambda$, where ϵ_n are the expectation values of the self-consistent mean-field matrix [not quasiparticle (q.p.) energies].

In the last method for the determination of nuclear densities, correct separation energies were assured. A single-particle spherical well, including the central and spin-orbit potentials for neutrons and protons, was assumed. Proper order of s.p. levels is guaranteed by the form of the potential. Potential parameters were adjusted slightly to obtain the experimental separation energies, charge rms radii, and, if known, the neutron rms radii.

IV. RESULTS

In this section we discuss the partial antiproton absorption widths $\Gamma_n(A-1)$ and $\Gamma_p(A-1)$ for captures on a neutron and proton, respectively, which produce cold $(A-1)$ final nuclei. The sum of the two is denoted by $\Gamma(A-1)$. Experiments determine those partial widths relative to the total absorption width Γ^{tot} . The data collected in Table II consist of two such ratios: $\sigma_{A-1} = \Gamma(A-1)/\Gamma^{\text{tot}}$ and $\sigma_{np} = \Gamma_n(A-$

TABLE II. Comparison of nuclear models. Experimental and calculated results for σ_{A-1} and σ_{np} are given. Calculations for atomic orbitals weighted as in Table I are done with $R_{np} = 0.82$.

	Expt. [1]		AD		HF		HFB	
	σ_{A-1}	σ_{np}	σ_{A-1}	σ_{np}	σ_{A-1}	σ_{np}	σ_{A-1}	σ_{np}
^{58}Ni	0.098(8)	0.9(1)	0.11	0.90	0.110	0.785	0.110	0.781
^{96}Zr	0.161(22)	2.6(3)	0.12	4.9	0.125	2.54	0.117	2.40
^{96}Ru	0.113(17)	0.8(3)	0.10	1.7	0.099	0.944	0.099	0.955
^{130}Te	0.184(36)	4.1(1)	0.12	2.6	0.124	3.14	0.123	3.22
^{144}Sm	0.117(20)	< 0.4	0.09	1.9	0.094	1.38	0.092	1.36
^{154}Sm	0.121(20)	2.0(3)	0.10	5.1	0.110	3.34	0.106	2.96
^{176}Yb	0.241(40)	8.10(7)	0.12	4.8	0.111	3.23	0.109	3.50
^{232}Th	0.095(14)	5.4(8)	0.12	7.6	0.087	3.80	0.109	4.65
^{238}U	0.114(9)	6.0(8)	0.13	10	0.092	4.09	0.100	4.31

$-1)/\Gamma_p(A-1)$. The first one, σ_{A-1} , is a test for a description of the antiproton absorption. In particular it checks the weakest points: understanding of the final state interactions and knowledge of the initial atomic states of capture. If quantitative understanding is achieved, one can claim control over the region of nuclear surface where the neutron halo is measured. The halo itself is seen via the σ_{np} ratio.

A. σ_{A-1} ratios

A typical antiproton absorption scenario is visualized in Figs. 1(a) and 1(b), which contain some ingredients of formula (18) for the capture widths. The results given in Table I show σ_{A-1} calculated for some circular atomic orbits that are most likely to be the states of nuclear capture. The shapes of $(A-1)$ capture densities are determined by the angular momentum l , strong nuclear absorption, and P_{miss} and thus are rather independent of the normalization of the atomic wave functions, i.e., of n . Thus, these ratios are typical to all n states. With the angular momentum l increased by one unit, in particular from the ‘‘lower’’ to the ‘‘upper’’ and higher l states, the σ_{A-1} increases by about 20%. Thus, the experimental data exclude a sizable fraction of high l captures but seem less restrictive on the states with l lower than l_{lower} , where the calculated σ_{A-1} stabilizes. On the other hand, cascade calculations done in kaonic, hyperonic, and antiprotonic atoms [6,33] show that the nuclear capture from the latter, $l < l_{\text{lower}}$, is unlikely. Also, these calculations indicate an accumulation of the capture probability on two, or at most three, values of l . This result is consistent with our capture probabilities, given in Table I, and calculated under the extreme assumption that the $l = l_{\text{upper}} + 1$ circular level is fully occupied at some stage of the atomic cascade. On the other hand, calculations of Ref. [7] allow a broader distribution with a 20% share of the $l_{\text{upper}} + 1$ and higher l states and a 10% share of $l_{\text{lower}} - 1$ values. If that is the real situation, our results for σ_{A-1} and σ_{np} would rise typically by a factor of 1.05. This is the likely uncertainty of the calculations in Tables I and II due to poor knowledge of the capture orbits. One hopes to clarify some of these points by experimental measurements of the cascade intensities and absolute cascade intensities in the nuclei of interest [34].

The σ_{A-1} calculated with the AD and other models are consistent with most of the experimental data, shown in

Table II. This gives some confidence in the validity of the final and initial state description. However, there are two outstanding discrepancies: Te and Yb.

I. Special cases of ^{130}Te and ^{176}Yb

The first case is understood qualitatively, while the second one presents a point of specific interest. It is known experimentally [35] that a strong $E2$ mixing, i.e., coupling of the atomic and nuclear rotations, occurs in the upper level of the ^{130}Te atom. This stimulates absorption from the upper level as indicated in Table I, and induces an effect of alignment of the nuclear and atomic spins in the states admixed to the upper level. Thus the orbital antiproton stays closer to the elongated part of the nucleus, as compared to states of equally averaged orientations. Thus, the final pions have a better chance to miss the nucleus. Calculations yield some 20% enhancement of the total absorption widths due to this effect [35]. One expects similar enhancement of the σ_{A-1} rate. It is also likely that the n/p ratio is higher at the poles of this nucleus.

The strong $E2$ mixing happens also in ^{176}Yb for high atomic orbits with $n=14$. It is not clear as yet what are the consequences for the atomic cascade process between the $n=14$ state and nuclear absorption. It is also not clear what correlation of the atomic motion and nuclear orientation is induced by this effect. Future experimental and theoretical studies [34] will help to elucidate this point.

Antiproton absorption in the heaviest elements ^{232}Th and ^{238}U is accompanied by nuclear fission of the final $(A-1)$ nuclei which, in principle, may affect the σ_{A-1} rate. However, in such nuclei, the radiative rates dominate the fission rates for excitations less than the neutron emission threshold [36]. In the even-odd nuclei of interest this domination is even stronger. Thus, the fission channel is expected to change σ_{A-1} only a little, and this is apparently borne out by the data in Table II.

B. σ_{np} ratios

The partial absorption widths are proportional to the effective absorptive amplitudes $\text{Im}t_{N\bar{N}}$ for the $\bar{p}n$ and $\bar{p}p$ pairs. These are not well known, although some average values follow from the optical potential phenomenology. The number required for neutron halo studies is a ratio $R_{np} = \text{Im}t(\bar{p}n)/\text{Im}t(\bar{p}p)$ which may be taken from other experiments. One value $R_{np} = 0.63$ has been obtained by Bugg *et al.* [3], from measurements of charged pions emitted in the \bar{p} absorption in carbon. Difficulties arise since it includes effects of final state mesonic interactions and the inherent uncertainties of the charge exchange reactions. This value of R_{np} generates mild disagreement with the data of Ref. [1] for all the nuclei and all nuclear models used here. The results given in Table I should be compared to the experimental data in Table II; similar discrepancies are generated by other models. A different result $R_{np} = 0.81(3)$ follows from the stopped antiproton absorption in deuterium [37]. This value is free from the pionic effects, but the deuteron kinematic conditions, in particular the binding energy, differ from those met at the nuclear surface. Another value of R_{np} obtained in ^4He is smaller and energy dependent. At rest, a number

$R_{np} = 0.48(10)$ has been deduced from rather involved analyses of the final state mesonic interactions in the three nucleon systems [38].

In this work we fix R_{np} from the best fit to our simplest nucleus ^{58}Ni . Our nuclear models yield similar results in this case and the fitted R_{np} is very close to the value obtained from the deuteron. We shall use the latter in our analysis.

The results for σ_{np} are collected in Table II. It is clear that the crudest model of asymptotic density strongly overestimates the ρ_n/ρ_p ratios at large distances. This property has been known already from the neutron pickup studies [10]. By the same effect, the AD model produces too large σ_{A-1} in the heaviest nuclei Th and U. The physics behind it is quite transparent.

(1) It is vital to have correct separation energies but these are not the whole story.

(2) The Coulomb barriers enhance the ρ_n/ρ_p ratio anomalously at large distances. That effect has to be offset by shell effects (angular momentum barriers) and correlations.

(3) Proper setting of the neutron skin defined in terms of mean squared radii $R_{\text{ms}}(\text{neutrons}) - R_{\text{ms}}(\text{protons})$ does not determine the ‘‘neutron halos.’’ The latter are understood here in terms of σ_{np} , i.e., ratios of high moments of density distributions.

What are the moments involved in the halos measured by the radiochemical experiment? For zero-range interactions and $P_{\text{miss}} = 1$ these are the ‘‘Barret moments,’’ i.e., $(2l)$ th moments due to centrifugal barriers corrected for the atomic wave functions. The P_{miss} and P_{dh} increase the order of the moments approximately by two units. On the other hand, the annihilation range effects, i.e., the folding, introduce moments smaller by two, four, and more units. The joint effect is best estimated by the dominant $2l$ density moment involved. As we see from Table II these are very high moments ranging from 10 in Ni to 18 in U.

The HF method with the SkP force gives roughly the correct neutron separation energies for (nearly) spherical systems ^{58}Ni , ^{96}Zr , and ^{144}Sm . It underbinds the last neutron in ^{96}Ru by 1.3 MeV but generally underestimates proton separation energies, e.g., by 1.1 MeV in ^{144}Sm and by 3 MeV in ^{58}Ni . This statement is qualitatively true also for the other deformed nuclei, with the one exception of ^{154}Sm , where the last neutron is underbound by 2.9 MeV. As we have checked in a separate calculation, the Skyrme force SIII does not improve the description of the Fermi energies in the studied nuclei.

Comparison of the data with the HF results shows clear disagreement for Yb and ^{144}Sm and a less pronounced disagreement for Te, Th, and U nuclei. On the basis of a comparison of calculated and experimental separation energies one can qualitatively expect corrections to the calculated σ_{A-1} and σ_{np} ratios (remembering that like errors in proton and neutron Fermi energies tend to compensate each other for the σ_{np}). In all the cases presented, except ^{144}Sm and ^{176}Yb , they go in the right direction.

In order to further understand the asymptotic HF densities one can look closer at how many orbitals contribute at large distances and test by means of the formula (14) the sensitivity of the ρ_n/ρ_p ratio to shifts in s.p. energies. In ^{58}Ni , at $r=7$ fm, two orbitals each give about 35% of the neutron density while three others give about 10% each. For protons,

there is one orbital contributing 56% (the highest one) and three other contributing about 12% each. At $r=15$ fm, the last occupied orbitals contribute 89% and 91% to the neutron and proton densities, respectively. Of course, the heavier the nucleus, the farther the asymptotic region and the more orbitals contribute to one-body densities in the range 8–15 fm. In ^{144}Sm , at $r=7$ fm, four states contribute more than 10% each to the neutron density (the highest percentage being 24%); four others contribute more than 5% each. Even at 15 fm, there are still four neutron orbitals contributing significantly to ρ_n (32%, 24%, 20%, and 16%), the reason being that their s.p. energies differ by not more than 4 MeV. In ^{238}U , at 15 fm, one must account for four neutron orbitals while only two proton orbitals contribute 79% and 15% to the ρ_p . Clearly, it is not only the distance r but also the (sub)shell structure which decides how many orbitals contribute.

In order to estimate the effect of s.p. energies on the density ratio ρ_n/ρ_p we have used the following procedure. Contributions to the density at $r=8$ fm were used as data and the extension to $r=15$ fm was performed using Eq. (19), with account for the Coulomb barrier. The resulting densities for ^{96}Zr are then larger than the exact HF densities roughly by a factor 7/4 and 9/7 for neutrons and protons, respectively. (The ρ_n/ρ_p ratio is then 161 instead of 115.) This error comes from the influence of the polynomial w_l in Eq. (19) but we concentrate on the effect of changing s.p. energies on the calculated ρ_n/ρ_p at $r=15$ fm. A decrease of the neutron energies by 1 MeV changes this ratio to 94, a decrease of the proton energies by 1 MeV increases the ratio to 234, and the simultaneous decrease of both proton and neutron energies by 1 MeV slightly decreases the ratio to 137. This gives some feeling as to the sensitivity of the ρ_n/ρ_p to the neutron and proton binding energies.

1. Special case of ^{58}Ni

This is our reference nucleus. The input data is certain and all model calculations produce consistent results. We use $R_{\text{ms}}(n)=3.734$ fm and $R_{\text{ms}}(p)=3.710$ fm [29], which in the s.p. approach produce $\sigma_{A-1}=1.05$ and $\sigma_{np}=0.88$. These ratios are close to the HF and HFB results from Table II. The latter two methods are not perfect: The HF method underbinds protons by 0.5 MeV and neutrons by 0.3 MeV. These errors are of no significance, however, since the absorption is spread over four neutron and four proton s.p. states.

2. Special case of ^{144}Sm

This nucleus displays a proton halo. Qualitatively, it might be due to the closed neutron shell. The separation energy of neutrons is large (10.6 MeV) compared with a small (6.2 MeV) one for the protons. However, this proton halo effect is not reproduced in our calculations. Both results for σ_{np} given in Table II and plots of the *neutron/proton* density ratios given in Fig. 2 indicate a neutron excess at the surface. The separation energies in our nuclear models are either fitted to the experimental (AD or s.p.) or well reproduced for neutrons. For protons the HF model underestimates the experimental value by 0.9 MeV and that should even enhance the proton tail over the real one. This case

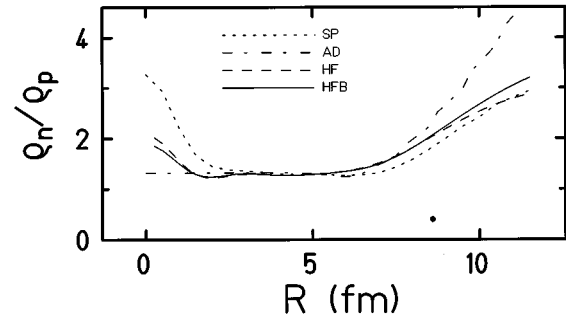


FIG. 2. The ratios of neutron and proton densities calculated with several nuclear models in the ^{144}Sm nucleus. Dashed line, HF; dotted line, s.p.; dot dashed line, AD; solid line, HFB. The $(A-1)$ “cold” absorption density peaks at 8.6 fm marked with a dot while its bulk is located between 7.2 and 10.2 fm. The experimental $\sigma_{np} < 0.4$.

indicates again that it is not only the separation energy that matters for the nuclear tail. The experimental result in ^{144}Sm is not understood and opens the case for more exotic speculations.

One obvious effect of inclusion of pair correlations is a change in the ρ_n/ρ_p ratio in the tail of the density following from the change in the Fermi energy. At smaller distances, however, this ratio may change in the opposite direction if levels other than the last one contribute to the density. It turns out that in all the cases studied the change in the ρ_n/ρ_p due to pairing is small up to 14 fm. A much more pronounced pairing effect on both ratios σ_{np} and σ_{A-1} comes from the P_{dh} factor which, e.g., in ^{232}Th changes from 0.52 (no pairing) to 0.69 (with pairing) at the total absorption peak at $r=8$ fm. This change more than balances a decrease in ρ_n/ρ_p ratio, providing for larger values of $\sigma_{A-1}=0.109$ and $\sigma_{np}=4.65$ (see Table II). The same P_{dh} factor is responsible for an increase of both ratios in ^{238}U , to 0.100 and 4.31, respectively, while the smaller P_{dh} leads to smaller σ_{A-1} and σ_{np} in ^{96}Zr (0.117 and 2.40, respectively). Pairing changes also σ_{A-1} for ^{154}Sm to 0.106 and σ_{np} for ^{154}Sm and ^{176}Yb to 2.96 and 3.50, respectively. Changes due to pairing are nearly zero for other nuclei.

V. CONCLUSIONS

The radiochemical method, which detects the products of nuclear capture of antiprotons, is a valuable source of information on the relative *neutron/proton* density distribution on the extreme tail of nuclear surface. The main features which we want to stress are the following.

(1) The nuclear regions tested are more peripheral than those studied by the x-ray measurements in hadronic atoms. One measures essentially the $2l$ moments of the density distributions where l is the angular momentum of “upper levels.” These moments are as high as 18 in the heaviest nuclei.

(2) There are special cases of alignment of nuclear and atomic angular momenta formed by the $E2$ mixing which display higher n/p ratios and higher rates of cold single-nucleon captures. These may test the composition of the pole regions in deformed nuclei. Further studies are recommended.

(3) The uncertainty in the initial atomic state of capture is kept under a fair control by the σ_{A-1} rates. However, additional x-ray experiments would be helpful to clarify this question.

(4) Strong neutron halos are observed in heavy deformed nuclei. These are not determined by the binding energies and Coulomb barriers alone. The shell effects (angular momentum) are also important. A few (two or three) of the highest nucleon orbitals contribute most to the cold capture rates.

(5) An interesting case of a proton halo is found in ^{144}Sm . It is not understood in terms of single-particle models, and may signal strong nuclear correlations in the surface region.

(6) Apart from the ^{144}Sm case the nuclear models reproduce the qualitative features of the observed halos.

ACKNOWLEDGMENTS

We thank J. Jastrzębski for his constant interest and collaboration and P.E. Hodgson for his advice and for arranging the collaboration that was kindly supported by The Royal Society and KBN. One of the authors (S.W.) gratefully acknowledges support by The Polish Committee for Scientific Research (KBN), Grant No. 2 P302 010 07.

-
- [1] J. Jastrzębski, H. Daniel, T. von Egidy, A. Grabowska, Y.S. Kim, W. Kurcewicz, P. Lubiński, G. Riepe, W. Schmid, A. Stolarz, and S. Wycech, Nucl. Phys. **A558**, 405c (1993); P. Lubiński, J. Jastrzębski, A. Grochulska, A. Stolarz, A. Trzcińska, W. Kurcewicz, F.J. Hartmann, W. Schmid, T. von Egidy, J. Skalski, R. Smolańczuk, S. Wycech, D. Hilscher, D. Polster, and H. Rossner, Phys. Rev. Lett. **73**, 3199 (1994).
- [2] D.H. Wilkinson, Philos. Mag. **4**, 215 (1959); P.B. Jones, *ibid.* **3**, 33 (1958).
- [3] W.M. Bugg, G.T. Condo, E.L. Hart, H.O. Cohn, and R.D. McCulloch, Phys. Rev. Lett. **31**, 475 (1973).
- [4] D.H. Davis, S.P. Lovell, M. Csejthey-Barth, J. Sacton, G. Schorochoff, and M. O'Reilly, Nucl. Phys. **B1**, 434 (1967).
- [5] E.H.S. Burhop, Nucl. Phys. **B1**, 438 (1967); **B44**, 445 (1972).
- [6] C.E. Wiegand and G.L. Godfrey, Phys. Rev. A **9**, 2284 (1974); R. Seki and C.E. Wiegand, Annu. Rev. Nucl. Sci. **25**, 241 (1975).
- [7] P. Roberson, T. King, R. Kunselman, J. Miller, R.J. Powers, P.D. Barnes, R.A. Eisenstein, R.B. Sutton, W.C. Lam, C.R. Cox, M. Eckhouse, J.R. Kane, A.M. Rushton, W.F. Vulcan, and R.E. Welsh, Phys. Rev. C **5**, 1954 (1977).
- [8] Th. Köhler, P. Blüm, G. Büche, A.D. Hancock, H. Koch, A. Kreissl, H. Poth, U. Raich, D. Rochmann, G. Backenstoss, Ch. Findeisen, J. Repond, L. Tauscher, A. Nilsson, S. Carius, M. Suffert, S. Charalambus, M. Chardalas, S. Dedoussis, H. Daniel, T. von Egidy, F.J. Hartmann, W. Kanert, G. Schmidt, J.J. Reidy, M. Nicholas, and A. Wolf, Phys. Lett. B **176**, 327 (1986).
- [9] D. Rohmann *et al.*, Z. Phys. A **325**, 261 (1986).
- [10] H.J. Körner and J.P. Schiffer, Phys. Rev. Lett. **27**, 1457 (1971).
- [11] C.J. Batty, Nucl. Phys. **A372**, 433 (1981).
- [12] C.J. Batty, Phys. Lett. B **189**, 393 (1987).
- [13] E. Friedman and J. Lichtenstadt, Nucl. Phys. **A455**, 573 (1986).
- [14] A.M. Green and S. Wycech, Nucl. Phys. **A377**, 441 (1982).
- [15] A.M. Green and S. Wycech, Nucl. Phys. **A467**, 744 (1987).
- [16] T. Suzuki and H. Narumi, Nucl. Phys. **A426**, 413 (1984).
- [17] S. Adachi and H.V. von Geramb, Acta Phys. Aust. **37**, 627 (1985); Nucl. Phys. **A470**, 461 (1987).
- [18] O. Dumbrajs, H. Heiselberg, A.S. Jensen, A. Miranda, G.C. Oades, and J.M. Richard, Nucl. Phys. **A457**, 491 (1986).
- [19] J. Kronenfeld, A. Gal, and J.M. Eisenberg, Nucl. Phys. **A430**, 413 (1984).
- [20] D. Ashery, Nucl. Phys. **A355**, 385 (1980); D. Ashery, I. Navon, G. Azuleos, H.K. Walter, H.J. Pfeifer, and F.W. Schlepütz, Phys. Rev. C **23**, 2173 (1981).
- [21] J.P. Shiffer, Nucl. Phys. **A355**, 339 (1980).
- [22] J. Cugnon and J. Vandermeulen, Ann. Phys. (Paris) **14**, 49 (1989).
- [23] P. Armaneros *et al.*, Report No. CERN/PSCC/80-101, 1980.
- [24] L.C. Liu and C.M. Shakin, Phys. Lett. **78B**, 389 (1978).
- [25] J.N. Ginocchio, Phys. Rev. C **17**, 195 (1978).
- [26] H.R. Clover, R.M. DeVries, N.J. DiGiacomo, and Y. Yariv, Phys. Rev. C **26**, 2138 (1982); J. Roy *et al.*, in *Proceedings of the International Seminar on NN*, Syracuse, 1975, edited by T.E. Kaloqeropoulos and K. C. Wali (Syracuse University, Syracuse, 1975).
- [27] X. Campi and A. Bouyssy, Phys. Lett. **73B**, 263 (1978).
- [28] H. Bethe and Ph. Siemens, Nucl. Phys. **B21**, 587 (1970).
- [29] G.R. Satchler and W.G. Love, Phys. Rep. C **55**, 183 (1979).
- [30] N.N. Bogolyubov, JETP Sov. Phys. **7**, 41 (1958); Usp. Fiz. Nauk **67**, 549 (1959) [Sov. Phys. Usp. **2**, 236 (1959)].
- [31] P. Ring and P. Schuck, *The Nuclear Many-Body Problem* (Springer-Verlag, New York, 1980).
- [32] J. Dobaczewski, H. Flocard, and J. Treiner, Nucl. Phys. **A422**, 103 (1984).
- [33] Y. Eisenberg and D. Kessler, Phys. Rev. **130**, 2352 (1961); A.D. Martin, Nuovo Cimento **27**, 1359 (1963); M. Leon and R. Seki, Phys. Rev. Lett. **32**, 132 (1973).
- [34] The CERN proposal, Experiment PS 209.
- [35] S. Wycech, F.J. Hartmann, H. Daniel, W. Kanert, H.S. Plendl, T. von Egidy, J.J. Reidy, M. Nicholas, L.A. Redmond, H. Koch, A. Kreissl, H. Poth, and D. Rohmann, Nucl. Phys. **A561**, 607 (1993).
- [36] J.A. Wheeler, in *Handbook of Physics*, edited by E.U. Condon and H. Odishow (McGraw-Hill, New York, 1958), p. 177.
- [37] R. Bizzari, P. Guidoni, F. Marcelija, F. Marzano, E. Castelli, and M. Sessa, Nuovo Cimento A **22**, 225 (1974); T.E. Kaloqeropoulos, Phys. Rev. D **22**, 2585 (1980).
- [38] F. Balestra *et al.*, Nucl. Phys. **A491**, 572 (1989).